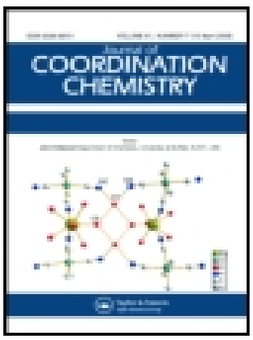

Journal of Coordination Chemistry

ISSN: 0095-8972 (Print) 1029-0389 (Online) Journal homepage: http://www.tandfonline.com/loi/gcoo20

Ruthenium(II) complexes of aroylhydrazones: Structural, electrochemical and electrostatic interactions with DNA

Jatinder Kaur, Madhura Damle, Hemant Mande, Prasanna Ghalsasi, Rajendra Kondedeshmukh, Parbati Bandyopadhyay & Rajeev Chikate

To cite this article: Jatinder Kaur, Madhura Damle, Hemant Mande, Prasanna Ghalsasi, Rajendra Kondedeshmukh, Parbati Bandyopadhyay & Rajeev Chikate (2017): Ruthenium(II) complexes of aroylhydrazones: Structural, electrochemical and electrostatic interactions with DNA, Journal of Coordination Chemistry, DOI: 10.1080/00958972.2017.1307344

To link to this article: http://dx.doi.org/10.1080/00958972.2017.1307344

Publisher: Taylor & Francis
Journal: *Journal of Coordination Chemistry*
DOI: http://dx.doi.org/10.1080/00958972.2017.1307344

Ruthenium(II) complexes of aroylhydrazones: Structural, electrochemical and electrostatic interactions with DNA

JATINDER KAUR†‡, MADHURA DAMLE†, HEMANT MANDE§, PRASANNA GHALSASI§, RAJENDRA KONDEDESHMUKH‡, PARBATI BANDYOPADHYAY*‡ and RAJEEV CHIKATE*†

†Department of Chemistry, Post-graduate and Research Center, MES AbasahebGarware College, Pune, India
‡Department of Chemistry, Fergusson College, Pune, India
§Department of Chemistry, Faculty of Science, The Maharaja Sayajirao University of Baroda, Vadodara, India

Four Ru(II) complexes with tridentate ligands *viz*. (4-hydroxy-N'-(pyridin-2-yl-ethylene) benzohydrazide $[Ru(L^1)(PPh_3)_2(Cl)]$ (**1**), N'-(pyridin-2-yl-methylene) nicotinohydrazide $[Ru(L^2)(PPh_3)_2(Cl)]$ (**2**), N'-(1H-imidazol-2-yl-methylene)-4-hydroxybenzohydrazide $[Ru(L^3)(PPh_3)_2(Cl)]$ (**3**) and N'-(1H-imidazol-2-yl-methylene) nicotinohydrazide $[Ru(L^4)(PPh_3)_2(Cl)]$ (**4**) have been synthesized and characterized. The methoxy-derivative of L^3H (abbreviated as **L^3H***) exists in *E* configuration with torsional angle of 179.4° around C_7-N_8-N_9-C_{10} linkage. Single crystal structures of acetonitrile coordinated ruthenium complexes of **1** and **3** $[Ru(L^1)(PPh_3)_2(CH_3CN)]Cl$ (**1a**) and $[Ru(L^3)(PPh_3)_2(CH_3CN)]Cl$ (**3a**) revealed tridentate ligands with significantly distorted octahedral geometry constructed by imine nitrogen, heterocyclic nitrogen and enolate amide oxygen, forming a *cis*-planar ring with *trans*-placement of two PPh_3 groups and a coordinated acetonitrile. Ligands (L^1H-L^4H) and their ruthenium complexes (**1**-**4**) are characterized by ^1H, ^{13}C, ^{31}P NMR and IR spectral analysis. Ru(II) complexes have reversible to quasi-reversible redox behavior with Ru(II)/Ru(III) oxidation potential of 0.40 – 0.71 V. The DNA binding constants determined by absorption spectral titrations with Herring Sperm DNA (HS-DNA) reveal that **L^4H** and **1** interact more strongly than other ligands and Ru(II) complexes. Complexes **1**-**3** exhibit DNA cleaving activity possibly due to strong electrostatic interactions while **4** displays intercalation.

*Corresponding authors. Email: rajuchikate29@gmail.com (R. Chikate); Parbatib7@gmail.com (P. Bandyopadhyay)

Keywords: Ru(II) complexes; Crystal structures; Aroylhydrazones; DNA binding; DNA cleavage

1. Introduction

Biological activities of metal complexes with bioactive ligands is a challenging task for designing of compounds with specific medicinal properties [1]. Metal-based anticancer agents is one such area where focus is centered as an alternative to *cis*-platin which has several side-effects like marrow suppression, hair loss, nephrotoxicity, nausea, vomiting and does not exhibit activity against several types of cancers. In this regard, ruthenium complexes possess promising activity plausibly due to Ru(II)/Ru(III) redox characteristics as well as beneficial photo-physical properties [2]. These complexes possess potential immune-suppressive [3], antimalarial [4], antioxidant [5], antibacterial [6], antifungal [7] and antiviral [8] properties. Successful phase I clinical trials for lung and colorectal tumors with Ru(III)-complexes of N-donor heterocycles NAMI-A (imidazolium *trans*-imidazole dimethylsulfoxide tetrachlororuthenate) and KP1019 (indazolium *trans*-tetrachlorobis(1*H*-indazole)ruthenate) have exhibited excellent anti-proliferative activity [9, 10]. This can be attributed to their ligand-exchange kinetics similar to platinum complexes [11], variable oxidation states (II – IV) under physiological conditions [12], high coordination number [13], ability to mimic iron in binding to biological molecules for transportation into tumor cells [14], activation by reduction of Ru(III) to Ru(II) for DNA binding in hypoxic and acidic environment in tumor cells [15], greater resistance to hydrolysis [16] and different binding modes with DNA [17]. NAMI-A exhibited significantly greater activity than *cis*-platin on metastases of the non small-cell lung carcinoma H460M2 cell line transplanted into severe combined immune deficient (SCID) mice [18]. Recently, ruthenium(II) complexes of flavanone ligands have displayed good pro-apoptotic activity against *cis*-platin resistant cancer sublineEJcisR [19]. Thus, it is imperative to design Ru(II) complexes that exhibit better anticancer activity and therefore, may be considered as an alternative to *cis*-platin.

Aroylhydrazones are biologically important pharmacophoric moieties (CO-NH-N=CH) containing different donor sites and strong tendency towards chelation with transition metals [20-22]. For example, 2-phenylindole-3-carbaldehyde benzoylhydrazones [23] inhibit the growth of MDA-MB-231 (M.D. Anderson - metastatic breast) and MCF-7 (Michigan Cancer Foundation-7) adenocarcinoma breast cancer cells. DNA cleaving activity is reported for ruthenium

complexes with ligands like 2-(2-pyridyl)-benzimidazole [24], polypyridyl [25], 2-phenyl-azo-imidazole [26] and benzoyl pyridine furoic acid hydrazone [27]. Thus, it is possible that synthesis of ruthenium complexes with aroylhydrazones may lead to enhanced DNA binding and cleaving properties.

In the present work, four new Ru(II) complexes with different aroylhydrazone ligands (scheme 1) are synthesized and characterized. Their DNA binding behavior is explored by spectroscopic titration and DNA cleavage activity using gel-electrophoresis with HS-DNA.

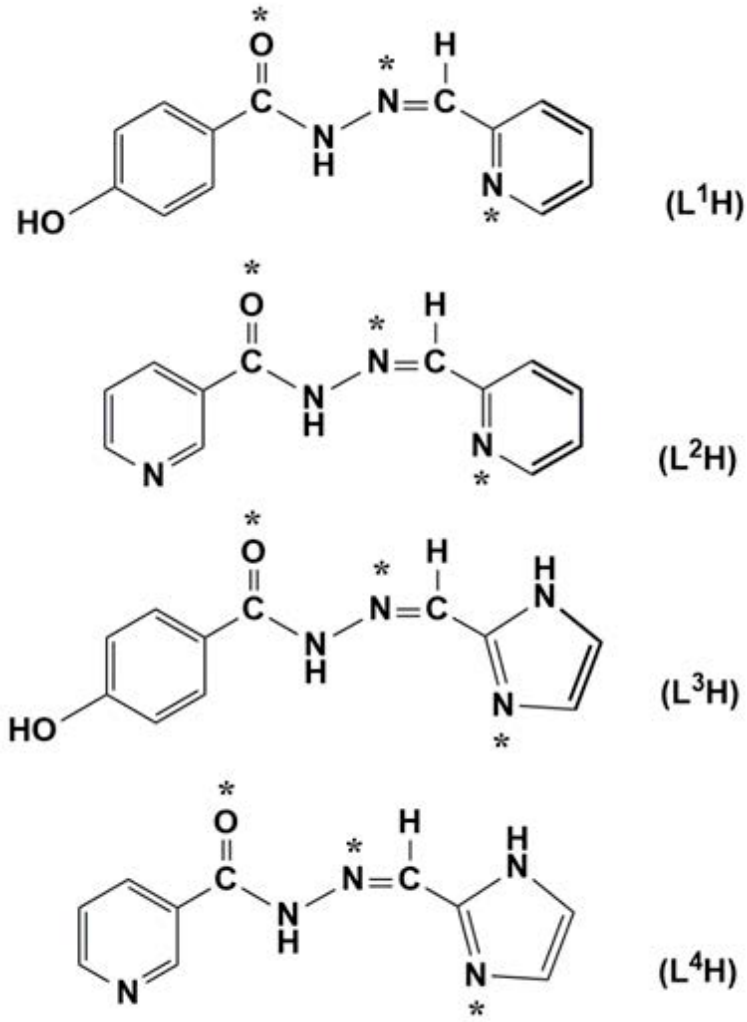

Scheme 1. Ligand structures L^1H – L^4H.

2. Experimental

2.1. *Materials and physical measurements*

All starting materials were used without purification: 4-hydroxybenzohydrazide, nicotinic acid hydrazide, pyridine-2-aldehyde, imidazole-2-carboxaldehyde and ruthenium(III) chloride trihydrate were all procured from Aldrich. $Ru(PPh_3)_3Cl_2$ was prepared as per the procedure reported [28]. Tetra ethyl ammonium perchlorate (TEAP) used for electrochemistry was prepared as reported [29]. All solvents used were of AR grade and used as received. For spectroscopic work, HPLC Grade solvents (Aldrich) were used. Plasmid pBR322 and gel loading dye was obtained from GeNei, ex-herring sperm from SRL, Agarose from Himedia, Tris base from Fischer Scientific and EDTA from Qualigens.

2.2. *Physical measurements and instrumentation*

Elemental analyses were carried out using a Perkin-Elmer 240 C, H and N Analyzer. Infrared spectra were recorded on a Bruker FT-IR spectrophotometer from 4000-400 cm^{-1} using KBr pellets. ^{1}H, ^{13}C and ^{31}P NMR spectra of ligands and complexes were recorded in DMSO-d_6 on a Bruker Ultrashield 400 MHz spectrometer with TMS and 84% H_3PO_4 as internal standards. Electronic spectra in solution were recorded on a Lambda 25, Perkin-Elmer spectrophotometer using DMSO as the solvent. Conductivity measurements of the complexes were carried out on a Digital Conductivity Meter (Systronics, Model 304). A CH1106A potentiostat was used for cyclic voltammetric experiments in DMSO solutions of the complexes containing 0.1M TEAP as supporting electrolyte. Three electrode system comprised of platinum working and auxiliary electrode and Ag-AgCl/saturated KCl as reference electrode. The potentials were calibrated against the ferrocene/ferrocenium couple.

2.3. *Synthesis of aroylhydrazones*

To a solution of 1 ml pyridine-2-aldehyde (1.07 g, 10 mmol) in 25 ml methanol, a methanolic solution (25 ml) of 4-hydroxy benzohydrazide (1.52 g, 10 mmol) was added dropwise with constant stirring. The reaction mixture was refluxed for 4 h with constant stirring upon which a solid was obtained, filtered, washed with cold methanol and diethyl ether and re-crystallized using methanol. This ligand is abbreviated as $\mathbf{L^1H}$. Similar procedure was followed for the synthesis of $\mathbf{L^2H}$ - $\mathbf{L^4H}$ (scheme 1).

Attempts to grow single crystals of $\mathbf{L^3H}$ were unsuccessful; instead its methoxy derivative was obtained from slow evaporation of methanolic mother liquor solution of its copper complex ***[au: OK?]***. Since the crystal structure confirmed it to be methoxy derivative of $\mathbf{L^3H}$, it is abbreviated as $\mathbf{L^3H^*}$.

$\mathbf{L^1H}$: Yield; 80%; ^{1}H NMR (DMSO-d_6) δ (ppm): 11.89 (s, 1H, NH), 10.24 (s, 1H, OH), 8.40 (s, 1H, CH=N), 8.42-6.88 (m, 8H, aromatic protons). ^{13}C NMR (DMSO-d_6) δ (ppm): 163.40 (C=O), 161.24 (C-OH), 147.70 (azomethine carbon), 115.42-153.72 (aromatic carbons). IR (KBr, cm^{-1}): 3212 (ν_{O-H}), 3065 (ν_{N-H}), 1641 ($\nu_{C=O}$), 1608 ($\nu_{C=N}$), 1560 $(\nu_{C=N})_{ring}$, 1066(ν_{N-N}). Anal. Calcd. for $C_{13}H_{11}N_3O_2$ (%): C, 64.72; H, 4.60; N, 17.42. Found: C, 64.22; H, 4.72; N, 17.34.

$\mathbf{L^2H}$: Yield; 71%; ^{1}H NMR (DMSO-d_6) δ (ppm): 12.24 (s, 1H, NH), 8.46 (s, 1H, -CH=N), 9.09-7.43 (m, 8H, aromatic protons). ^{13}C NMR (DMSO-d_6) δ (ppm):162.42 (C=O), 148.84 (azomethine carbon), 120.41-153.50 (aromatic carbons). IR (KBr, cm^{-1}): 3055 (ν_{N-H}), 1660 ($\nu_{C=O}$), 1593 ($\nu_{C=N}$), 1561 $(\nu_{C=N})_{ring}$, 1069 (ν_{N-N}). Anal. Calcd. for $C_{12}H_{10}N_4O$ (%): C, 63.71; H, 4.46; N, 24.77. Found: C, 64.02; H, 4.21; N, 23.94.

$\mathbf{L^3H}$: Yield; 74%; ^{1}H NMR (DMSO-d_6) δ (ppm): 12.82 (s, 1H, NH), 11.66 (s, 1H, NH), 10.34 (s, 1H, OH), 8.34 (s, 1H, CH=N), 7.8-6.86 (m, 6H, aromatic protons). ^{13}C NMR (DMSO-d_6) δ (ppm): 163.51 (C=O), 162.52 (C-OH), 144.54 (azomethine carbon), 113.52-141.62 (aromatic carbons). IR (KBr, cm^{-1}): 3233 (ν_{O-H}), 3055 (ν_{N-H}), 1652 ($\nu_{C=O}$), 1610 ($\nu_{C=N}$), 1587 $(\nu_{C=N})_{ring}$, 1070(ν_{N-N}). Anal. Calcd. for $C_{11}H_{10}N_4O_2$ (%): C, 57.39; H, 4.34; N, 24.34. Found: C, 58.02; H, 4.38; N, 24.61.

$\mathbf{L^4H}$: Yield: 81%; ^{1}H NMR (DMSO-d_6) δ (ppm): 12.91 (s, 1H), 12.00 (s, 1H), 8.26 (s,1H, CH=N), 9.09-7.10 (m, 6H, six aromatic protons). ^{13}C NMR (DMSO-d_6) δ (ppm): 161.00 (C=O), 147.00 (azomethine carbon), 115.41-146.54 (aromatic carbons). IR (KBr, cm^{-1}): 3037 (ν_{N-H}), 1658 ($\nu_{C=O}$), 1616 ($\nu_{C=N}$), 1591 $(\nu_{C=N})_{ring}$, 1054 (ν_{N-N}). Anal. Calcd. for $C_{10}H_9N_5O$ (%): C, 55.81; H, 4.18; N, 32.55. Found: C, 55.34; H, 4.52; N, 32.78.

2.4. *Synthesis of ruthenium(II) complexes*

To a hot methanolic (20 ml) solution of L^1H (0.12 g, 0.5 mmol), Et_3N (0.06 ml, 0.5 mmol) was added dropwise and the mixture was stirred for 10 min. To this solution, 0.48 g (0.5 mmol) $Ru(PPh_3)_3Cl_2$ dissolved in 10 mL was added and the solution was refluxed for 4 h under N_2. A

reddish-brown crystalline precipitate thus obtained was collected by filtration, washed with cold methanol and dried under vacuum. Similar procedure was adopted for synthesis of other complexes (scheme 2). These ruthenium complexes prepared with different ligands are abbreviated as **1** (L^1H), **2** (L^2H), **3** (L^3H) and **4** (L^4H). The reddish brown crystals of **1** and **3** were obtained by slow diffusion of n-hexane into acetonitrile solution. X-ray structures of **1** and **3** showed exchange of coordinated chloride ligands with acetonitrile molecules and are referred as **1a** and **3a** in Section 3.1. It is quite likely that during crystallization, chloride ions may be replaced with acetonitrile molecules as these crystals are obtained after keeping this solution for almost one month. The molar conductivities of these complexes in DMSO (10^{-3} M) demonstrate that they are electrolytes with conductance of 26.0-38.9 Ω^{-1} cm^2mol^{-1}.

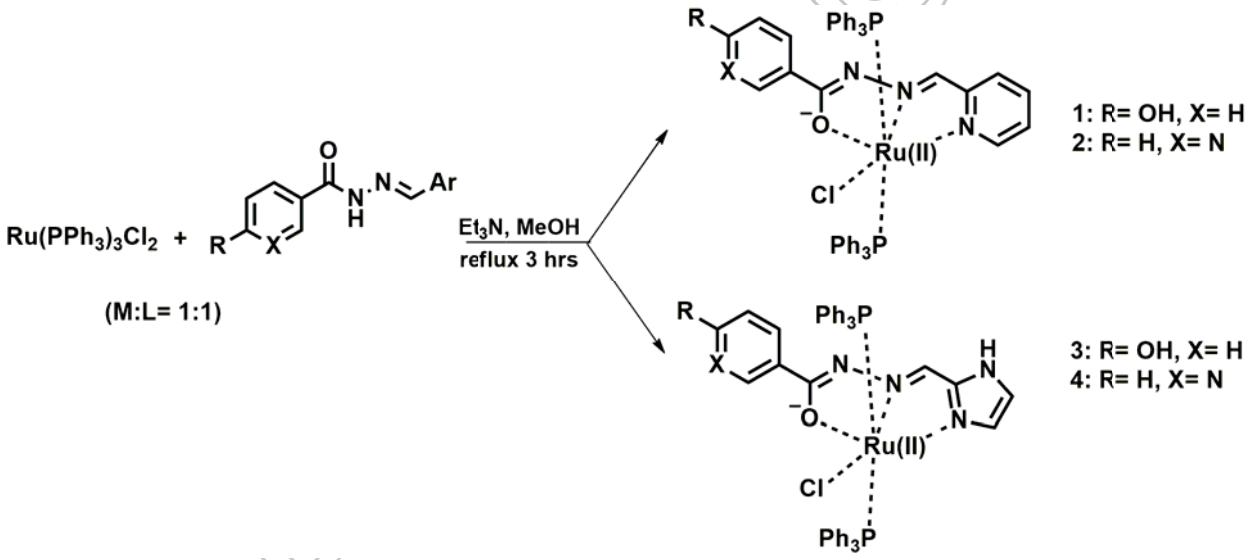

Scheme 2. Schematic representation for the syntheses of **1**-**4**.

1; **$[Ru(PPh_3)_2(L^1)Cl]\cdot H_2O$**: Yield; 46%; ^{1}H NMR (DMSO-d_6) δ (ppm): 9.94 (s, 1H, OH), 8.35-6.69 (m, aromatic and one azomethine protons). ^{13}C NMR (DMSO-d_6) δ (ppm): 127.90-137.10 (aromatic and azomethine carbons). ^{31}P NMR (DMSO-d_6) δ (ppm): 24.56 (s). IR (KBr, cm^{-1}): 3278 (ν_{O-H}), 3055 (ν_{N-H}), 1593 ($\nu_{C=N}$), 1480 $(\nu_{C=N})_{ring,}$ 1279 (ν_{C-O}), 1093 (ν_{N-N}), 742, 694, 516 (ν_{PPh3}). Anal. Calcd. for $RuC_{49}H_{42}ClN_3O_3P_2$ (%): C, 64.01; H, 4.57; N, 4.57. Found: C, 63.84; H, 4.36; N, 4.55.

2; **[Ru(PPh$_3$)$_2$(L^2)Cl]·H$_2$O**: Yield; 56%; ^{1}H NMR (DMSO-d$_6$) δ (ppm): 7.63-7.14 (m, aromatic and azomethine protons). ^{13}C NMR (DMSO-d$_6$) δ (ppm): 128.00-136.92 (aromatic and azomethine carbons). ^{31}P NMR (DMSO-d$_6$) δ (ppm): 24.11 (s). IR (KBr, cm^{-1}): 3057 (ν_{N-H}), 1585 ($\nu_{C=N}$), 1481 ($\nu_{C=N}$)$_{ring}$, 1188 (ν_{C-O}), 1090 (ν_{N-N}), 743, 696, 518 (ν_{PPh3}). Anal. Calcd. for $RuC_{48}H_{41}ClN_4O_2P_2$ (%): C, 63.75; H, 4.53; N, 6.19. Found: C, 64.15; H, 4.43; N, 6.11.

3; **[Ru(PPh$_3$)$_2$(L^3)Cl]·H$_2$O**: Yield; 54%; ^{1}H NMR (DMSO-d$_6$) δ (ppm): 9.85 (s, 1H, OH), 7.57-7.20 (m, aromatic and azomethine protons). ^{13}C NMR (DMSO-d$_6$) δ (ppm): 129.10-133.70 (aromatic and azomethine carbons). ^{31}P NMR (DMSO-d$_6$) δ (ppm): 26.15 (s). IR (KBr, cm^{-1}): 3260 (ν_{O-H}), 3056 (ν_{N-H}), 1591 ($\nu_{C=N}$), 1481 ($\nu_{C=N}$)$_{ring}$, 1277 (ν_{C-O}), 1092 (ν_{N-N}), 743, 695, 517(ν_{PPh3}). Anal. Calcd. for $RuC_{47}H_{41}ClN_4O_3P_2$ (%): C, 62.1; H, 4.51; N, 6.17. Found: C, 62.30; H, 4.61; N, 6.26.

4; **[Ru(PPh$_3$)$_2$(L^4)Cl]·H$_2$O**: Yield; 41%; ^{1}H NMR (DMSO-d$_6$) δ (ppm): 7.61-7.20 (m, aromatic and azomethine protons). ^{13}C NMR (DMSO-d$_6$) δ (ppm): 128.00-137.14 (aromatic and azomethine carbons). ^{31}P NMR (DMSO-d$_6$) δ (ppm): 23.51 (s). IR (KBr, cm^{-1}): 3058 (ν_{N-H}), 1585 ($\nu_{C=N}$), 1481 ($\nu_{C=N}$)$_{ring}$, 1188 (ν_{C-O}), 1087 (ν_{N-N}), 742, 696, 518 (ν_{PPh3}). Anal. Calcd. for $RuC_{46}H_{40}ClN_5O_2P_2$ (%): C, 61.49; H, 5.12; N, 8.96. Found: C, 61.8; H, 4.95; N, 8.36.

2.5. *Single crystal X-ray diffraction studies*

The crystal data for **L^{3}H***, **1a** and **3a** were collected at 298 K on Xcalibur, Eos and Gemini diffractometers. CuK$_\alpha$ radiation (λ) 1.54184 Å for **L^{3}H*** and **1a** and Mo Kα radiation (λ) 0.71073 Å for **3a** were used as X-ray source. The data reductions were performed with CrysAlisPro, data collection and data reduction software package (Oxford Diffraction Ltd., Abingdon, UK). Structure of **1a** was solved using Olex2 [30] by direct methods with SIR2004 structure solutions programme [31] and refined with ShelXH-1997 [32]. The single crystal structures of **L^{3}H*** and **3a** were solved with the Superflip structure solution program [33] using Charge Flipping and refined with the ShelXL refinement package using least squares minimization. The ORTEP views of **L^{3}H***, **1a** and **3a** are shown in figures 1, 2 and 3, respectively. The crystallographic data and significant bond lengths and angles are summarized in tables 1, 2 and 3.

2.6. *DNA Binding studies*

The possible binding modes of the ligands and their Ru(II) complexes with DNA were studied by UV-VIS absorption titration. The binding experiments were carried out at room temperature in TRIS-HCl buffer, pH 7.5 at fixed concentration of ruthenium complexes (25 µM) to which increments of DNA stock solution are added. The absorbance ratio of herring sperm DNA (HS-DNA) at 260 and 280 nm was 1.80-1.85, which indicated that the DNA is free of protein impurities. The concentration of the HS-DNA was calculated spectrophotometrically using the molar absorption coefficient (6600 $M^{-1}cm^{-1}$) at 260 nm. The DNA concentration was varied from 0-60 µM. The reaction mixture was incubated for 5 minutes before recording the spectra. The intrinsic binding constant for the Ru(II) complexes can be determined by monitoring the changes in absorbance at fixed wavelength and calculated by the following equation,

$$[DNA]/[\varepsilon_a - \varepsilon_f] = [DNA]/[\varepsilon_b - \varepsilon_f] + 1/K_b[\varepsilon_b - \varepsilon_f]$$

where [DNA] is the concentration of DNA in the base pairs. The apparent absorption coefficients ε_a, ε_f and ε_b correspond to A_{obs}/[Ru], the extinction coefficient for the free and bound forms of compounds, respectively. The slope and Y intercept of the linear fit of [DNA] / $[\varepsilon_a - \varepsilon_f]$ versus [DNA] give $1/[\varepsilon_a - \varepsilon_f]$ and $1/K_b[\varepsilon_b - \varepsilon_f]$, respectively. The intrinsic binding constant K_b can be obtained from the ratio of the slope to the Y intercept [34-36].

2.7. *DNA Cleavage studies*

DNA cleaving ability of the metal complexes was determined by agarose gel electrophoresis in accord with established protocols. The pBR322 plasmid DNA was used as the substrate for DNA cleavage. Reactions were set using 300 ngpBR322 in 50 mM TRIS-HCl, 10 mM NaCl buffer of pH 8 with 200 µM of ligands and their ruthenium complexes. The reaction mixtures were incubated at 37 °C for 18 h. These samples were analyzed by electrophoresis on 1% agarose (containing 0.5 µg/ml EB) in TAE buffer (40 mM TRIS-acetate, 1 mM EDTA pH 8.0) at 70V. The images were captured and analyzed on Gel Doc system. The efficiencies of the complexes to cleave DNA were determined by ability to convert super coiled pBR322 into nicked circular and linear [37]. Proper controls were maintained during experiments.

3. Results and discussion

3.1. *Crystal structure description of the ligand and Ru(II) complexes*

The crystal of $\mathbf{L^3H^*}$ crystallizes in a monoclinic space group with four crystallographically independent molecules in the unit cell (figure 1). It is obtained as the methoxy derivative of $\mathbf{L^3H}$. Similar work has been reported [38] where Cu(II) mediates nucleophilic attack of methoxide at the polarized azomethine carbon to form an imidate. The molecule exists in the *E* conformation around N8-N9 bond with torsion angle close to 180° for C7-N8-N9-C10 bonds [39]. The bond distances of 1.232 and 1.346 Å for O13-C7and N8-C7 are consistent with the keto form of the amide functionality [38]. N9-C10 bond length of 1.278 Å is typical for azomethine C=N group.

1a and **3a** crystallize in the monoclinic space group $P2_1/c$ as shown in figures 2 and 3. Summary of crystallographic data is presented in table 2. These complexes form octahedral geometry through heterocyclic nitrogen, azomethine nitrogen, *trans*-placed P from triphenylphosphine, acetonitrile and deprotonated amide oxygen of mono-anionic tridentate $\mathbf{L^1}$ and $\mathbf{L^3}$ ligands. The observed bond angles of 169.4° and 169.22° for P1–Ru01–P2 and P8–Ru1–P27 bonds indicate appreciable distortion within the structures of **1a** and **3a** as evident from deviation of ~ 11° from idealized bond angle of 180°. Such a departure is plausibly induced by constrained five member NN and NO chelate rings formed around ruthenium(II) by hydrazone ligands with a bite angle of 79.8° and 76.4° for **1a** and 79.2° and 76.6° for **3a**, respectively [40]. The Ru-N, Ru-O, Ru-P bond distances for **1a** and **3a** are similar to the one reported for polypyridine and pyrazole complexes [41]. Binding of O51 with Ru1 via enolization is observed from an increase in C-O bond length from 1.232 Å for $\mathbf{L^3H}$* (C7-O13) to 1.291 Å for **3a** (C47-O51). **1a** and **3a** exist in *E* configuration around the N-N bond as evident from C3-N1-N2-C43 and C47-N48-N49-C50 torsion angles of 179.2° and 178.8°, respectively (Supporting Information, table T1). Almost identical coordination sphere of $\mathbf{L^1}$ and $\mathbf{L^3*}$ around Ru(II) implies that these ligands possess comparable ligand field strengths as revealed from Ru-N bond distances.

3.2. *Spectral analysis*

Infrared spectra of the ligands display $\nu_{C=O}$ stretch of 1660-1641 cm^{-1} which disappear upon complexation with Ru(II) due to its enolization with concomitant appearance of C-O vibrations at 1277-1188 cm^{-1}. The coordination of azomethine nitrogen is evident from shift of moderately

strong band at 1593-1616 cm^{-1} in ligands to lower energy (1585-1593 cm^{-1}) in these complexes [42-45]. The substantial downward shift of ~100 cm^{-1} for ring nitrogen ($\nu_{C=N}$) from 1560-1591 cm^{-1} to ~1480 cm^{-1} supports coordination of heterocyclic nitrogen to ruthenium. The broad bands at 3212-3055 cm^{-1} for hydrazones and their Ru(II) complexes are attributed to ν_{O-H} and ν_{N-H} vibrations. Triphenylphosphine coordination [46] is confirmed by the presence of three strong bands at 743, 696 and 518 cm^{-1}.

The coordination modes of the ligands to Ru(II) are further confirmed from ^{1}H NMR spectra of the ligands and their complexes in DMSO-d_6 (Supporting Information, figures S1-S8). The multiplets observed for aromatic protons of benzhydrazone and triphenyl phosphine at 6.69-8.35 ppm for both ligands and Ru(II) complexes suggests that these protons are not directly affected by the presence of ruthenium [47]. Similar effect is also observed for azomethine C-H protons at 8.26-8.46 for **L^1H - L^4H** that seems to be overlapped with the aromatic region. A sharp singlet at 11.66-12.24 ppm for amide proton of free ligand is absent in these complexes due to enolization of amide oxygen. ^{13}C NMR spectra of **L^1H - L^4H** exhibits peaks at 161.00-163.51 ppm due to carbonyl carbon while they are not observed for **1**-**4** due to enolization of the amide (Supporting Information, figures S9-S16). On the other hand, sharp peaks at 24.56, 24.11, 26.15 and 23.51 ppm for ^{31}P NMR spectra of **1** (figure 4) and **2**-**4** (Supporting Information, figures S17-S19) indicate structurally equivalent *trans* placement of phosphines [48], an observation already established by X-ray crystal structure.

Electronic spectra of Ru(II) complexes exhibit absorption bands at 256-427 nm (Supporting Information, figure S20). The high intensity bands at 256-344 nm are assigned to intra-ligand π-π^* and n-π^* transitions occurring within the ligand which are shifted to lower energy upon complexation [49]. Due to unsymmetrical donor environment around Ru(II), the characteristic d-d transitions are not observed; instead only one MLCT band could be located between 412-487 nm [50-52].

3.3. *Electrochemistry*

The electrochemical behavior for **1**-**4** is examined in DMSO by cyclic voltammetric measurements (table 4); a representative CV curve is depicted in figure 5. All these complexes exhibit metal centered oxidative response in the range 0.40 – 0.71 V due to Ru(II)/Ru(III) redox couple. Peak current ratios approaching one are observed for all the complexes, which clearly

suggest one electron redox process ($i_{pa}/i_{pc}\approx1$). They possess $E_{1/2}$ values that are close to those observed for Ru(II) complexes with similar types of ligands [53, 54]. Lower oxidation potential observed for **2** and **4** is due to the presence of two heterocyclic rings that influence the electronic structure of these complexes and the ease at which they can be oxidized. Except for **2**, the other complexes display reversible one electron transfer with a peak-to-peak separation of 40-60 mV. For **1**, this reversible process is further ascertained by scan rate dependence studies (figure 5, inset). The peak potential difference increases as scan rate is increased due to facile Ru(II)/Ru(III) redox process probably induced by heterocyclic nitrogen present in $\mathbf{L^1H}$. The lower oxidation potentials for **2** and **4** are probably due to exchange of coordinated chloride with the DMSO as observed with single crystal structural analysis of **1a** and **3a** where chloride ion is replaced by acetonitrile. Such an exchange between chloride and DMSO could not be established by ^{1}H NMR spectral analysis.

3.4. *DNA binding studies*

3.4.1. Electronic absorption studies. DNA binding capacity of $\mathbf{L^1H}$ - $\mathbf{L^4H}$ is monitored between 300-340 nm that corresponds to intra-ligand π-π* and n-π* transitions (Supporting Information, figures S21-S24). Such interactions lead to either hypochromic or hyperchromic shifts originating from structural changes for DNA [55]. The hypochromic shift refers to intercalative interaction along with red shift in the band while hyperchromic shift is associated with only electrostatic interactions. $\mathbf{L^4H}$ exhibits excellent binding capacity as evident from significant increase in the absorbance for DNA as well as appreciably higher K_b value (6.7×10^5 M^{-1}) while $\mathbf{L^3H}$ seems to be less active towards DNA binding (Supporting Information, table T2). It can be argued that presence of heterocyclic nitrogen of $\mathbf{L^4H}$ significantly contributes toward electrostatic interactions at the major groove of DNA. Thus, the order of binding affinity of ligands to DNA is $\mathbf{L^4H}$>$\mathbf{L^1H}$ >$\mathbf{L^2H}$>$\mathbf{L^3H}$.

1-**4** exhibited interesting results with DNA binding capacities when monitored between 260-340 nm (figure 6); **2** and **3** display almost similar hyperchromic shifts while **4** shows hypochromic shift. However, **1** possesses both hyper- and hypochromic shifts at lower (< 25 μmoles) and higher (> 25 μmoles) DNA concentrations, respectively. Such features can be attributed to significant structural changes within DNA due to both intercalative and electrostatic interactions for **1** as compared to other complexes [36, 56]. It implies that the structure of **1** is

more flexible so as to bind efficiently with DNA at both major and minor grooves and therefore exhibits better binding capacity. The intrinsic binding constant K_b for **1**-**3** are in the range of 2-3 × 10^5 M^{-1} (Supporting Information, table T3) that are comparable to those reported for Ru(II) complexes [57-63].

3.4.2. DNA cleavage studies. DNA cleavage efficiency of **L^1H - L^4H** and their Ru(II) complexes is evaluated by agarose gel electrophoresis (figure 7). Supercoiled plasmid DNA (SC; form I) migrates relatively faster than nicked circular (NC; form II) and linear plasmid (LC; form III). Single stranded nick in the plasmid DNA generates slow moving NC plasmid while double stranded break in the DNA causes its linearization that exhibits intermediate mobility on electrophoresis [64]. DMSO used as solvent does not have any significant effect on DNA cleaving activity as both SC and NC forms of plasmid are observed (Lane 9) which is similar to control (Lanes 1 and 7). The restriction enzyme EcoRI cleaves pBR322 DNA giving single linearized band (LC; Lanes 2 and 8). The interaction of **L^1H**, **L^2H** and **L^4H** with plasmid leads to decrease in the intensity of SC and increase in NC (Lanes 6, 5 and 12) as well as cleaving of double strands thereby generating LC. However, **L^3H** exhibits similar behavior to the control suggesting that it does not possess DNA cleaving activity (Lane 10). It is further corroborated with DNA binding capacity except for **L^3H**; all other ligands exhibit better binding capability.

Complexes **2**, **3** and **4** display all three forms of the plasmid DNA (Lanes 4, 11 and 13) while cleavage pattern for **1** shows absence of the SC along with substantial presence of NC with small amount of linearization (Lane 3). Compared to **L^1H**, **1** is more active as evident from complete disappearance of the SC band. The band pattern for **2** is similar to that of the **L^2H** which implies that there is no effect of ruthenium on the cleaving activity. **3** exhibits higher DNA cleavage compared to **L^3H** as evident from presence of NC and SC forms along with a faint linear band suggesting its fragmentation. The disappearance of linear band for **4** can be attributed to intercalation which is further corroborated with hypochromic shift observed for DNA binding [65]. These results are supportive of DNA cleavage that also can be evaluated from intrinsic binding constants K_b for **1**-**3** that favor electrostatic binding to DNA leading to nick in the strand as observed in the cleavage pattern. The electrostatic interaction of the complexes with DNA thus enhances the nuclease like activity converting SC to NC and further causing linearization of the plasmid. However, **L^4H** exhibits good electrostatic binding while **4**

exhibits intercalative mode of interaction with DNA that can be prominently seen in the DNA cleavage pattern with loss of the LC band for **4**.

4. Conclusion

Four Ru(II)-hydrazone complexes with triphenyl phosphine as ligands are synthesized, characterized and their DNA interaction studies reported. Tridentate aroylhydrazones coordinate *meridonial* with *trans* placement of triphenyl phosphine ligands in a distorted octahedral geometry. These complexes exhibit Ru(II)/Ru(III) redox couple at fairly positive oxidation potential having reversible nature. DNA binding studies suggest that aroylhydrazone ligands bind through strong electrostatic attractions due to presence of heterocyclic ring while their complexes exhibit hyper and hypo-chromic shifts suggesting their binding affinity towards both minor and major grooves. The DNA binding constants (K_b) of **1**-**3** are in agreement with other Ru(II) complexes reported. Interaction of ligands with plasmid DNA leads to increase in nicked circular form as well as cleaving of double strands, thereby generating linear strands. Such behavior is also observed for the complexes with **1** exhibiting better interaction probably due to the reversible Ru(II)/Ru(III)couple. Presence of two heterocyclic rings within the ligand structure account for such behavior.

Disclosure statement

No potential conflict of interest was reported by the authors.

Acknowledgements

Authors thank Dr. Rupam Dinda, NIT Rourkela and Dr. Shyamal Chattopadhyay, BESU, Kolkata for analytical support.

Funding

PB is grateful to University Grants Commission, New Delhi for financial assistance [Grant No. 41-216/2012]. RC and MD thank Department of Science and Technology for DST-FIST infrastructural Grant.

References

[1] B.J. Pages, D.L. Ang, E.P. Wright, J.R. Aldrich-Wright. *Dalton Trans*., **44**, 3505 (2015).

[2] M.R. Gill, J.A. Thomas. *Chem. Soc. Rev*., **41**, 3179 (2012).

[3] E. de Paula Silveira-Lacerda, C.A.S.T. Vilanova-Costa, F. de Castro Pereira, A. Hamaguchi, L.A. Pavanin, L.R. Goulart, M.I. Homsi-Brandenburgo, A.M. Soares, W. Bastista dos Santos, A. Nomizo. *Biol. Trace Elem. Res*., **133**, 270 (2010).

[4] E. Ekengard, L. Glans, I. Cassells, T. Fogeron, P. Govender, T. Stringer, P. Chellan, G. C. Lisensky, W.H. Hersh, I. Doverbratt, S. Lidin, C. Kock, P.J. Smith, G.S. Smith, E. Nordlander. *Dalton Trans*., **44**, 19314 (2015).

[5] Z. Li, Z. Liang, H. Huang, Y. Liu. *J. Mol. Struct*., **1001**, 36 (2011).

[6] F. Li, J.G. Collins, F.R. Keene. *Chem. Soc. Rev*., **44**, 2529 (2015).

[7] A. Anthonysamy, S. Balasubramanian, V. Shanmugaiah, N. Mathivanan. *Dalton Trans*., 2136 (2008).

[8] C.S. Allardyce, P.J. Dyson, D.J. Ellis, P.A. Salter, R. Scopelliti. *J. Organomet. Chem*., **35**, 668 (2003).

[9] A. Bergamo, C. Gaiddon, J.H.M. Schellens, J.H. Beijnen, G. Sava. *J. Inorg. Biochem*., **106**, 90 (2012).

[10] M. Groessl, E. Reisner, C.G. Hartinger, R. Eichinger, O. Semenova, A.R. Timerbaev, M.A. Jakupec, V.B. Arion, B.K. Keppler. *J. Med. Chem*., **50**, 2185 (2007).

[11] Y.N.V. Gopal, D. Jayaraju, A.K. Kondapi. *Biochemistry*, **38**, 4382 (1999).

[12] E.S. Antonarakis, A. Emadi. *Cancer Chem. Pharm*., **66**, 1 (2010).

[13] V. Brabec, O. Novakova. *Drug Resist. Updates*, **9**, 111 (2006).

[14] S. David, R.S. Perkins, F.R. Fronczek, S. Kasiri, S.S. Mandal, R.S. Srivastava. *J. Inorg. Biochem*., **111**, 33 (2012).

[15] P. Schluga, C.G. Hartinger, A. Egger, E. Reisner, M. Galanski, M.A. Jakupec, B.K. Keppler. *Dalton Trans*., 1796 (2006).

[16] K.J. Kilpin, S.M. Cammack, C.M. Clavel, P.J. Dyson. *Dalton Trans*., **42**, 2008 (2013).

[17] R. Pettinari, F. Marchetti, C. Pettinari, A. Petrini, R. Scopelliti, C.M. Clavel, P.J. Dyson. *Inorg. Chem*., **53**, 13105 (2014).

[18] G. Sava, S. Zorzet, C. Turrin, F. Vita, M.R. Soranzo, G. Zabucchi, M. Cocchietto, A. Bergamo, S. DiGiovine, G. Pezzoni, L. Sartor, S. Garbisa. *Clin. Cancer Res*., **9**, 1898 (2003).

[19] M.M. Kasprzak, L. Szmigiero, E. Zyner, J. Ochocki. *J. Inorg. Biochem*., **105**, 518 (2011).

[20] B. Ghosh, S. Naskar, S. Naskar, A. Espinosa, S.C.K. Hau, T.C.W. Mak, R. Sekiya, R. Kuroda, S. Kumar Chattopadhyay. *Polyhedron*, **72**, 115 (2014).

[21] T. Liu, C. Sun, X. Xing, L. Jing, R. Tan, Y. Luo, W. Huang, H. Song, Z. Li, Y. Zhao. *Bioorg. Med. Chem. Lett*., **22**, 3122 (2012).

[22] S. Dash, A. Panda, R. Ramesh, S. Pasayat, S. Majumder, A. Biswas, W. Kaminsky, S. Mukhopadhyay, S. Bhutia, R. Dinda. *J. Inorg. Biochem*., **144**, 1 (2015).

[23] S. Vogel, D. Kaufmann, M. Pojarová, C. Müller, T. Pfaller, S. Kühne, P.J. Bednarski, E. Angerer. *Bioorg. Med. Chem*., **16**, 6436 (2008).

[24] M.M. Alonso, N. Busto, F.A. Jalón, B.R. Manzano, J.M. Leal, A.M. Rodríguez, B. García, G. Espino. *Inorg. Chem*., **53**, 11274 (2014).

[25] A. Srishailam, Y.P. Kumar, N.M.D. Gabra, P. Venkat Reddy, N. Deepika, N. Veerababu, S. Satyanarayana. *J. Fluores*., **23**, 897 (2013).

[26] U.K. Mazumder, M. Gupta, S.S. Karki, S. Bhattacharya, S. Rathinasamy, T. Sivakumar. *Bioorg. Med. Chem*., **13**, 5766 (2005).

[27] M. Alagesan, N.S.P. Bhuvanesh, N. Dharmaraj. *Dalton Trans*., **43**, 6087 (2014).

[28] T.A. Stephenson, G. Wilkinson. *J. Inorg. Nucl. Chem*., **28**, 945 (1966).

[29] D.T. Sawyer, A. Sobkowiak, J.L. Roberts Jr., Electrochemistry for Chemists, 2nd Edn., Wiley, New York, 36 (1995).

[30] O.V. Dolomanov, L.J. Bourhis, R.J. Gildea, J.A.K. Howard, H. Puschmann. *J. Appl. Cryst*., **42**, 339 (2009).

[31] M.C. Burla, R. Caliandro, M. Camalli, B. Carrozzini, G.L. Cascarano, L.D. Caro, C. Giacovazzo, G. Polidori, D. Siliqi, R. Spagna. *J. Appl. Cryst*., **40**, 609 (2007).

[32] G.M. Sheldrick. *Acta Cryst. A*, **64**, 112 (2008).

[33] L. Palatinus, G. Chapuis. *J. Appl. Cryst*., **40**, 786 (2007).

[34] M. Mishra, K. Tiwari, S. Shukla, R. Mishra, V.P. Singh. *Spectrochim. Acta, Part A*, **132**, 452 (2014).

[35] L. Tan, F. Wang, H. Chao, Y. Zhou, C. Weng. *J. Inorg. Biochem*., **101**, 700 (2007).

[36] Q. Zhen, Q. Zhang, J. Liu, B. Ye, L. Ji, L. Wang. *J. Inorg. Biochem.*, **78**, 293 (2000).

[37] P.U. Maheswari, M. Palaniandavar. *J. Inorg. Biochem.*, **98**, 219 (2004).

[38] N.R. Sangeetha, S. Pal, S. Pal. *Polyhedron*, **19**, 2713 (2000).

[39] K. Sampath, S. Sathiyaraj, G. Raja, C. Jayabalakrishnan. *J. Mol. Struct.*, **1046**, 82 (2013).

[40] R.N. Prabhu, R. Ramesh. *RSC Adv.*, **2**, 4515 (2012).

[41] S. David, R.S. Perkins, F.R. Fronczek, S. Kasiri, S.S. Mandal, R.S. Srivastava. *J. Inorg. Biochem.*, **111**, 33 (2012).

[42] R.M. Silverstein, F.X. Webster, *Spectrometric Identification of Organic Compounds*, 6th Edn., Wiley, New York, 101 (1998).

[43] K. Nakamoto, *Infrared and Raman Spectra of inorganic and Coordination Compounds*, 4th Edn., Wiley, New York, 242 (1986).

[44] N. Mathew, M.R.P. Kurup. *Spectrochim. Acta, Part A*, **78**, 1424 (2011).

[45] S. Mondal, S. Naskar, A.K. Dey, E. Sinn, E. Eribal, S.R. Herron, S.K. Chattopadhyay. *Inorg. Chim. Acta*, **398**, 98 (2013).

[46] F. Basuli, A.K. Das, G. Mostfa, S.M. Peng, S. Bhattacharya. *Polyhedron*, **19**, 1663 (2000).

[47] M.R. Maurya, S. Agarwal, M. Abid, A. Azam, C. Badder, M. Ebel, D. Rehder. *Dalton Trans.*, 937 (2006).

[48] I.N. Booysen, A. Adebisi, O.Q. Munro, B. Xulu. *Polyhedron*, **73**, 1 (2014).

[49] G. Raja, R.J. Butcher, C. Jayabalakrishnan. *Spectrochim. Acta, Part A*, **94**, 210 (2012).

[50] M. Haga, E.S. Dodsworth, A.B.P. Lever. *Inorg. Chem.*, **25**, 447 (1986).

[51] R. Raveendran, S. Pal. *Polyhedron*, **24**, 57 (2005).

[52] P. Sengupta, R. Dinda, S. Ghosh, W.S. Sheldrick. *Polyhedron*, **22**, 447 (2003).

[53] D. Mishra, S. Naskar, A.J. Blake, S. Chattopadhyay. *Inorg. Chim. Acta*, **360**, 2291 (2007).

[54] S. Naskar, S. Naskar, M.G.B. Drew, S.I. Gorelsky, B.L. Kaiser, A. Aukauloo, D. Mishra, S.K. Chattopadhyay. *Polyhedron*, **28**, 4101 (2009).

[55] K.M. Vyas, R.N. Jadeja, D. Patel, R.V. Devkar, V.K. Gupta. *Polyhedron*, **80**, 20 (2014).

[56] P.U. Maheswari, M. Palaniandavar. *Inorg. Chim. Acta*, **357**, 901 (2004).

[57] M. Mohanraj, G. Ayyannan, G. Raja, C. Jayabalakrishnan. *J. Coord. Chem.*, **69**, 3545 (2016).

[58] P. Kalaivani, R. Prabhakaran, F. Dallemer, K. Natarajan. *RSC Adv*., **4**, 51850 (2014).

[59] K. Jeyalakshmi, J. Haribabu, N. Bhuvanesh, R. Karvembu. *Dalton Trans*., **45**, 12518 (2016).

[60] R. Panah, H. Hadadzadeh, H. Farrokhpour, M. Mortazavi, Z. Amirghofran. *Inorg*. *Chim*. *Acta*, **454**, 184 (2017).

[61] C. Wang, Q. Wu, Y. Zeng, D. Huang, C. Yu, X. Wang, W. Mei. *J*. *Coord*. *Chem*., **68**, 1 (2015).

[62] F. Hayat, Z. Rehman, M.H. Khan. *J*. *Coord*. *Chem*., **70**, 279 (2017).

[63] J. Sun, W. Chen, X. Song, X. Zhao, A. Ma, J. Chen. *J*. *Coord*. *Chem*., **68**, 308 (2015).

[64] Y. Xie, G. Jiang, J. Yao, G. Lin, H. Huang, X. Wang, Y. Liu. *J*. *Coord*. *Chem*., **66**, 2423 (2013).

[65] J. Lu, Q. Sun, J. Li, L. Jiang, W. Gu, X. Liu, J. Tian, S. Yan. *J*. *Inorg*. *Biochem*., **137**, 46 (2014).

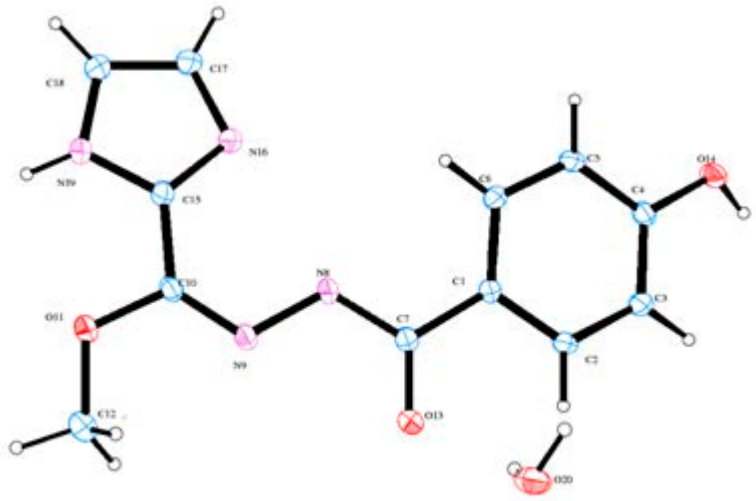

Figure 1. ORTEP diagram of $\mathbf{L^3H^*}$.

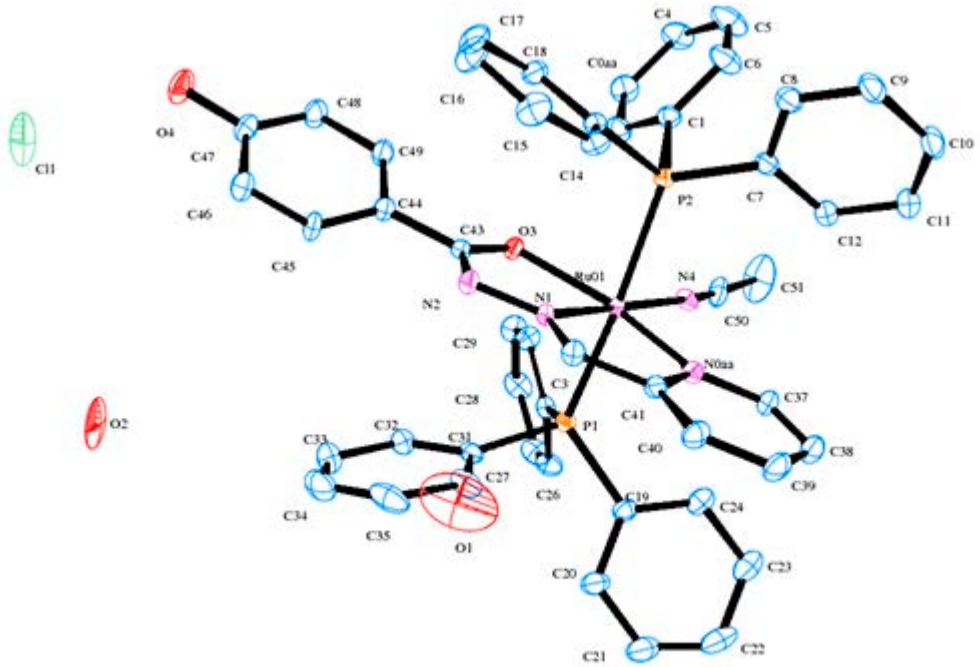

Figure 2. ORTEP diagram of **1a** $[Ru(PPh_3)_2(L^1)(CH_3CN)]Cl\cdot 2H_2O$.

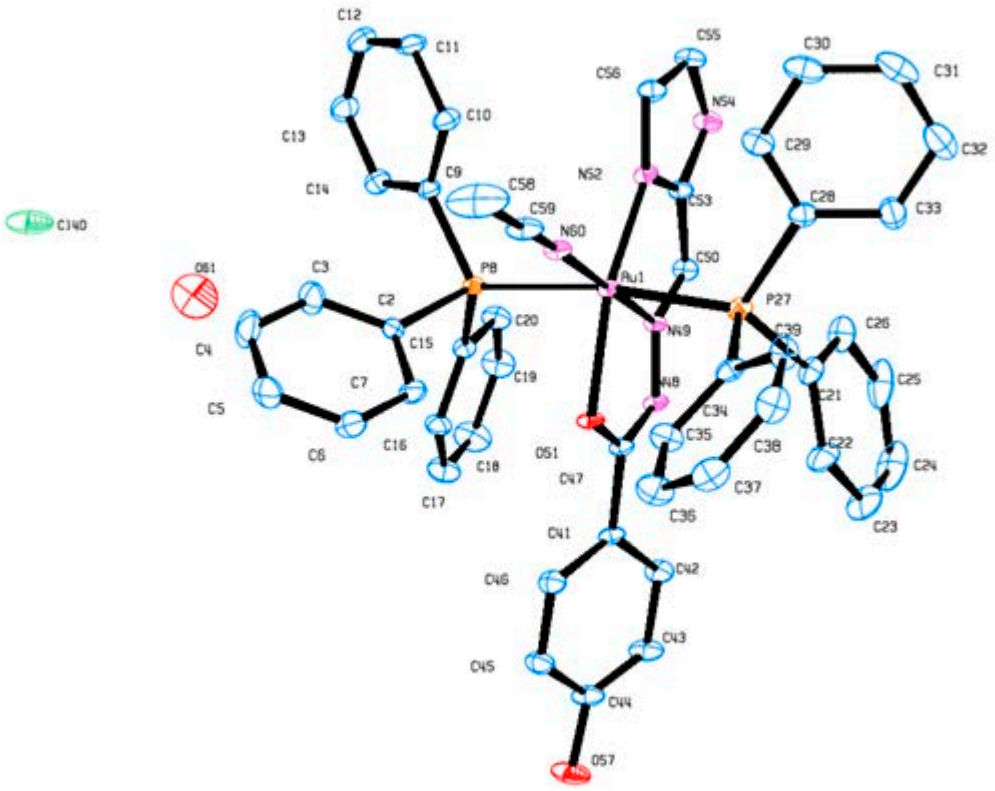

Figure 3. ORTEP diagram of **3a** $[Ru(PPh_3)_2(L^3)(CH_3CN)]Cl\cdot H_2O$.

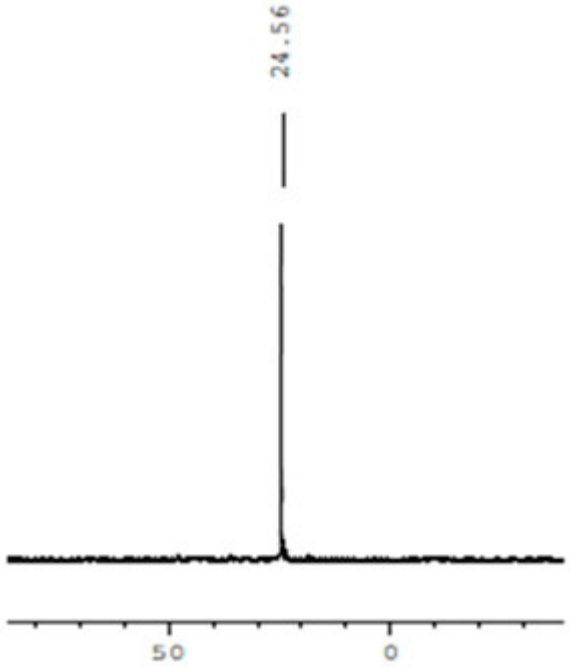

Figure 4. ^{31}P NMR spectra of **1**.

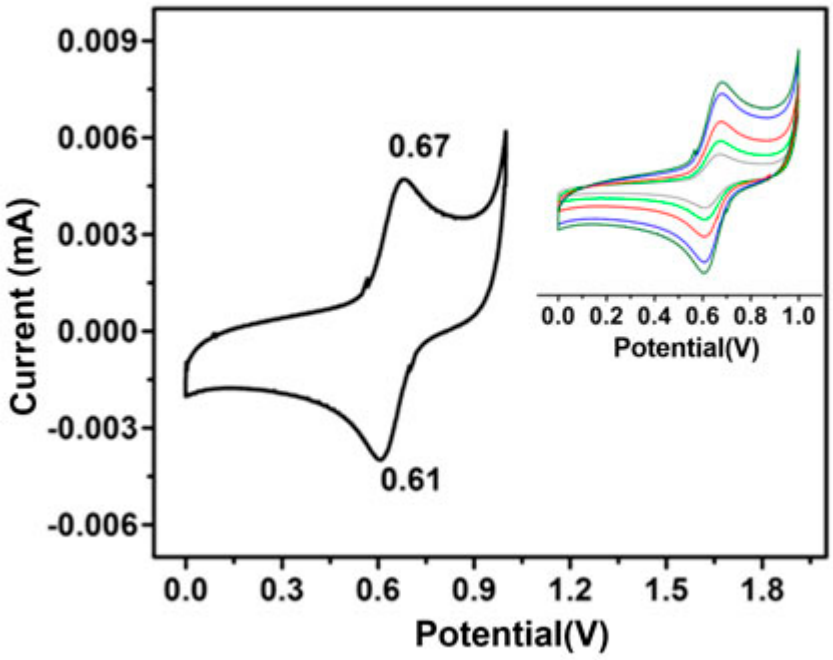

Figure 5. Cyclic voltammogram of **1** at 0.1 Vs^{-1} scan rate in DMSO with ferrocene as the internal reference; inset: scan rate dependence of **1** at different scan rates (0.05, 0.1, 0.2, 0.4, 0.5 Vs^{-1}).

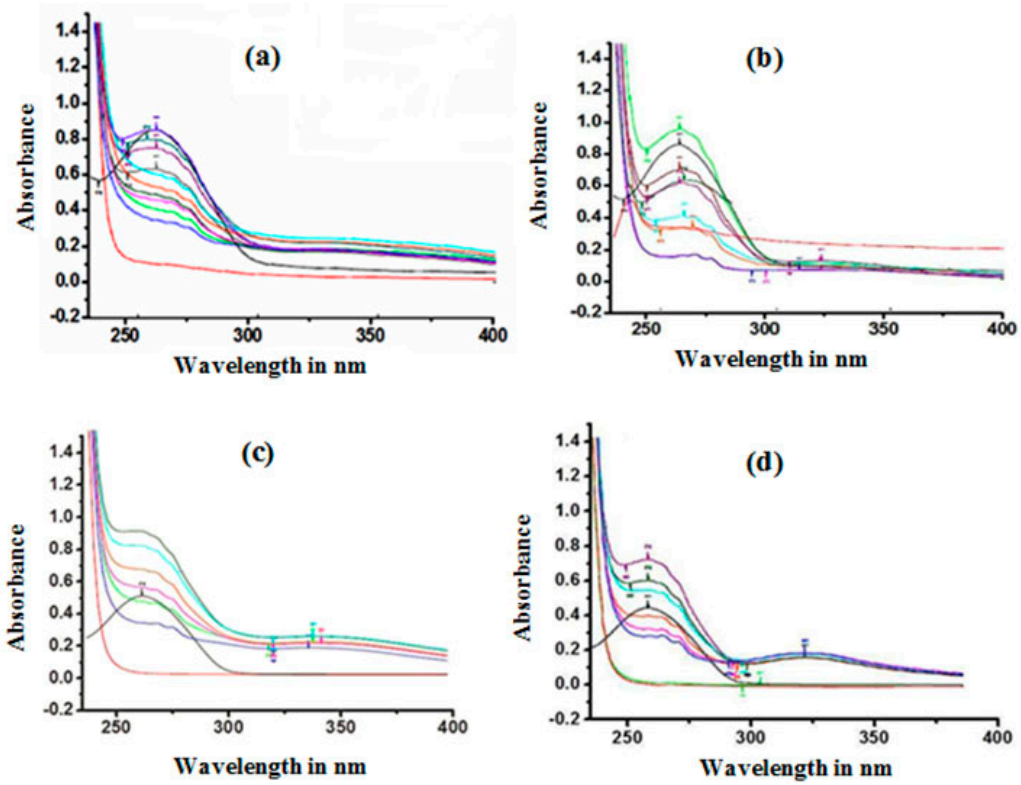

Figure 6. Absorption spectra of complexes (25 µM): (a) **1**, (b) **2**, (c) **3**, (d) **4** in absence and presence of increasing concentration of DNA (0-60 µM) at room temperature in Tris-HCl (pH 7.5).

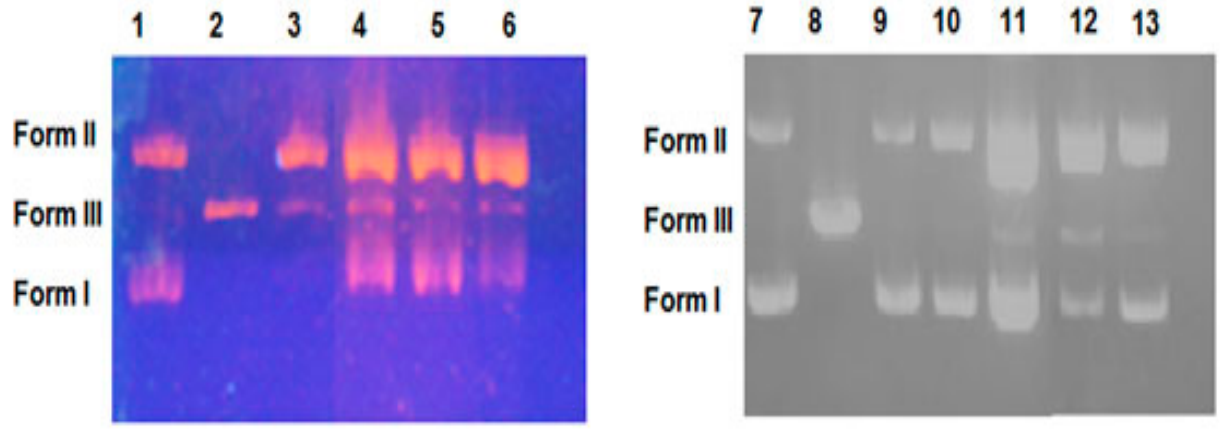

Figure 7. Agarose (1%) gel electrophoresis DNA cleavage patterns for **L^1H - L^4H** and **1-4** (200 µM). Lanes 1 and 7: pBR control; Lane 9: pBR + DMSO; Lanes 2 and 8: linearization of pBR with Eco-RI; Lane 3: **1**; Lane 4: **2**; Lane 5: **L^2H**; Lane 6: **L^1H**; Lane 10: **L^3H**; Lane 11: **3**; Lane 12: **L^4H**; Lane 13: **4**.

Table 1. Crystallographic data for $\mathbf{L^3H^*}$, **1** and **3**.

Identification code	$\mathbf{L^3H^*}$	**1**	**3***
CCDC number	1406574	1406575	---
Empirical formula	$C_{12}H_{13}N_4O_4$	$C_{102}H_{86}Cl_2N_8O_5P_4Ru_2$	$C_{49}H_{42}ClN_5O_3P_2Ru$
Formula weight	277.26	1900.71	949.34
Temperature/K	293	298	293(2)
Crystal system	Monoclinic	Monoclinic	Monoclinic
Space group	Cc	$P2_1/c$	$P2_1/c$
a/Å	4.45737(17)	10.77076(19)	10.4930(7)
b/Å	20.2121(6)	22.3029(5)	22.1551(17)
c/Å	14.9544(5)	20.8752(3)	20.8691(13)
α/°	90.00	90.00	90.00
β/°	97.912(4)	93.4536(15)	94.267(6)
γ/°	90.00	90.00	90.00
Volume/Å^3	1334.45(8)	5005.52(16)	4838.1(6)
Z	4	4	4
ρ_{calc} g/cm^3	1.380	1.261	1.303
μ/mm^{-1}	0.898	3.961	0.490
F(000)	580.0	1952.0	1948.0
Crystal size/mm^3	0.28 × 0.25 × 0.23	0.3 × 0.29 × 0.25	0.39 × 0.32 × 0.3
Radiation	CuKα (λ = 1.54184)	CuKα (λ = 1.54184)	MoKα (λ = 0.71073)
2Θ range for data collection/°	8.74 to 146.24	7.92 to 133.98	6.16 to 58.14
Index ranges	$-5 \le h \le 4$, $-24 \le k \le 24$, $-18 \le l \le 18$	$-13 \le h \le 8$, $-27 \le k \le 27$, $-25 \le l \le 25$	$-14 \le h \le 13$, $-30 \le k \le 26$, $-27 \le l \le 28$
Reflections collected	4474	37405	27054
Independent reflections	2676 (R_{int} = 0.0238)	8923 (R_{int} = 0.0757)	11258 (R_{int} = 0.0848)
Data / restraints / parameters	2676 / 2 / 190	8923 / 0 / 570	11258 / 0 / 553
Goodness-of-fit on F^2	1.073	1.090	1.074
Final R indexes [I>=2σ (I)]	R_1 = 0.0395 wR_2 = 0.0996	R_1 = 0.0669 wR_2 = 0.1796	R_1 = 0.1031 wR_2 = 0.2608
Final R indexes [all data]	R_1 = 0.0419 wR_2 = 0.1030	R_1 = 0.0801 wR_2 = 0.1871	R_1 = 0.1430 wR_2 = 0.2853
Largest diff. peak / hole /e Å^{-3}	0.30 / -0.24	1.59 / -0.63	4.20 / -1.28

*R-factor of **3** is high, hence data not submitted to CCDC

Table 2. Bond distances (Å) and angles (°) for $\mathbf{L^3H^*}$.

Bond distances (Å)		Bond angles (°)	
O13-C7	1.232(3)	O13-C7-C1	120.9(2)
N9-C10	1.278(3)	N8-N9-C10	116.3(2)
N8-C7	1.346(3)	N9-N8-C7	117.61(19)

Table 3. Bond distances (Å) and angles (°) for $[Ru(PPh_3)_2(L^1)(CH_3CN)]Cl\cdot 2H_2O$ (**1a**) and $[Ru(PPh_3)_2(L^3)(CH_3CN)]Cl\cdot H_2O$ (**3a**).

1a		**3a**	
Ru01-P1	2.3755(15)	Ru1-P8	2.3657(19)
Ru01-O3	2.132(4)	Ru1-O51	2.128(5)
Ru01-N1	1.960(4)	Ru1-N49	1.986(5)
Ru01-P2	2.3800(15)	Ru1-P27	2.374(2)
Ru01-N0AA	2.087(5)	Ru1-N52	2.094(6)
Ru01-N4	2.068(5)	Ru1-N60	2.046(6)
O3-C43	1.280(7)	O51-C47	1.291(8)
C43-N2	1.330(7)	C47-N48	1.335(9)
O3-Ru01-P1	88.05 (11)	O51-Ru1-P8	83.70(15)
N4-Ru01-O3	103.13(17)	O51-Ru1-N60	103.3(2)
N1-Ru01-P2	92.88(13)	N52-Ru1-P8	96.74(17)
N0AA-Ru01-P2	96.53(14)	N60-Ru1-P8	87.29(18)
N0AA-Ru01-N4	100.7(2)	N60-Ru1-N52	100.9(2)
N4-Ru01-P1	87.15(13)	N49-Ru1-P8	92.81(17)
P1-Ru01-P2	169.40(5)	P8-Ru1-P27	169.22(7)
O3-Ru01-N0AA	156.17(17)	O51-Ru1-N52	155.8(2)
N1-Ru01-N0AA	79.72(18)	N52-Ru1-N49	79.2(2)
O3-Ru01-N1	76.45(16)	N49-Ru1-O51	76.6(2)

Table 4. Cyclic voltammetric (298 K) data for Ru(II) complexes.

Compound	E_{pc}	E_{pa}	$E_{1/2}$/V[a]	ΔE_p/mV[b]	% i_{pc}/i_{pa}
1	+0.67	+0.61	+ 0.64	60	97
2	+0.49	+0.40	+ 0.445	90	96
3	+0.71	+0.67	+ 0.69	40	92
4	+0.45	+0.40	+ 0.425	50	100

[a]$E_{1/2}$ is calculated as the average of anodic (*E*pa) and cathodic (*E*pc) peak potential. [b]Δ*E*p=*E*pa−*E*pc.

Graphical abstract